

# Ruthenium Polypyridyl Complexes Containing a Conjugated Ligand $L_{DQ}$ ( $L_{DQ} = 1$ -[4-(4'-methyl)-2,2'-bipyridyl]-2-[4-(4'-N,N'-tetramethylene-2,2'-bipyridinium)]ethene): Synthesis, Characterization, and Photoinduced Electron Transfer at Solution–Zeolite Interfaces

Haoyu Zhang, Cheruvallil S. Rajesh, and Prabir K. Dutta\*

Department of Chemistry, 120 West 18th Avenue, The Ohio State University, Columbus, Ohio 43210

Received: July 11, 2008; Revised Manuscript Received: November 23, 2008

Photoinduced electron transfer from sensitizers attached to zeolite surface to electron acceptors within the zeolite provides opportunities for long-lived charge separation, as well as potential utilization of the charge separated species. In this study, the focus is on the ruthenium polypyridyl compound  $[(bpy)_2RuL_{DQ}]^{4+}$  (where bpy = bipyridine, and  $L_{DQ} = 1$ -[4-(4'-methyl)-2,2'-bipyridyl]-2-[4-(4'-N,N'-tetramethylene-2,2'-bipyridinium)]-ethene) and its unquaternized analogue of structural formula  $[(bpy)_2RuL]^{2+}$  ( $L = trans$ -1,2-bis[4-(4'-methyl)-2,2'-bipyridyl]ethene). Both complexes show strong metal-to-ligand charge-transfer (MLCT) and olefinic ligand based absorption bands. The emission of  $[(bpy)_2RuL_{DQ}]^{4+}$  in solution is quenched, whereas the  $[(bpy)_2RuL]^{2+}$  complex exhibits emission at 675 nm. The quenching is attributed to the intramolecular electron transfer from the Ru center to the diquat (DQ) moiety upon photoexcitation. The  $[(bpy)_2RuL_{DQ}]^{4+}$  complex is stable upon visible light illumination, while  $[(bpy)_2RuL]^{2+}$  is photochemically unstable. Nanocrystalline zeolite Y with particle size of  $\sim 80$  nm was prepared and characterized by diffraction and electron microscopy. Protonated  $[(bpy)_2RuL]^{2+}$  and  $[(bpy)_2RuL_{DQ}]^{4+}$  were attached to the surface of the zeolite Y by ion-exchange and permanent incorporation into the supercage, respectively. The zeolite-encapsulated  $[(bpy)_2RuL_{DQ}]^{4+}$  species was found to be emissive at 695 nm with a lifetime of 796 ns. Intermolecular electron transfer from photoexcited  $[(bpy)_2RuL_{DQ}]^{4+}$  to methylviologen ( $MV^{2+}$ ) in solution was not observed. However, in the zeolite,  $\sim 40\%$  of the initial  $MV^{+}$  generated via photoinduced electron transfer from surface-bound  $[(bpy)_2RuL_{DQ}]^{4+}$  survived for the duration of the experiment (milliseconds). The long-lived viologen radical resulted from a competitive effect between the back electron transfer from  $MV^{+}$  to  $Ru^{3+}$  ( $k_b = 3.0 \times 10^5 \text{ s}^{-1}$ ) with a self-exchange electron propagation between the densely packed viologens ( $k_{hop} = 2.0 \times 10^5 \text{ s}^{-1}$ ) that moves the charge away from the surface of the zeolite.

## Introduction

The key step in natural photosynthesis is photoinduced charge separation. Successful artificial photosynthetic strategies mimicking natural photosynthesis require molecular assemblies that exhibit long-lived photoinduced charge separation. The limiting issue in artificial photosynthesis is the back electron transfer between the photochemically generated redox pairs.<sup>1</sup> Heterogeneous supports are known to promote charge separation,<sup>2,3</sup> and aluminosilicate zeolites have shown considerable promise in this regard.<sup>4</sup> The arrangement of cages and channels in these crystalline zeolites allows for placement of molecules in well-defined spatial arrangements. Trisbipyridine ruthenium(II) as an electron donor and bipyridinium ions as electron acceptors have been extensively investigated<sup>5</sup> and serve as good models for evaluating the role of zeolite hosts in photochemical charge separation. Several studies have focused on the steady-state photochemistry of trisbipyridine ruthenium(II) and bipyridinium ions in zeolites, demonstrating the possibilities for the long-term charge separation.<sup>6,7</sup> Time-resolved diffuse reflectance spectroscopy has been used to examine the kinetics of the photoinduced electron transfer process for this system. With  $[Ru(bpy)_3]^{2+}$  ion-exchanged on the surface of methylviologen containing zeolite, it was found that the rate constant of the back electron transfer (BET) is considerably slower than that

for comparable systems in solution.<sup>8</sup> Using nanometer-sized zeolite X crystals as photochemical hosts, the BET from the bipyridinium radical to encapsulated  $[Ru(bpy)_3]^{3+}$  was also reported to be smaller by several orders of magnitude as compared to the forward reaction.<sup>9</sup> For high concentrations of bipyridinium ions in the zeolite, long-lived charge separation was observed because the photogenerated electron can migrate via electron hopping among adjacent bipyridinium molecules away from the ruthenium center.<sup>10</sup>

A large number of ruthenium polypyridine complexes have been investigated for applications related to the solar energy conversion.<sup>11</sup> The redox and excited-state properties can be tuned by changing the ligands or ligand substituents. Rigid ligands with extended  $\pi$ -conjugation systems tend to have longer excited-state lifetimes as a result of decreased bond displacement changes in the excited state.<sup>12,13</sup> An example of this kind of ligand is bbpe (bbpe =  $L = trans$ -1,2-bis[4-(4'-methyl)-2,2'-bipyridyl]ethene), and this rigid, conjugated ligand has been used to prepare mono- and dinuclear complexes with Ru and Os.<sup>12</sup> Recently, we have reported photoreactions of  $[(bpy)_2RuL]^{2+}$  containing bbpe.<sup>14</sup> It was found that dimerization and isomerization are triggered through a photoinduced electron transfer mechanism. The poor photostability of the complex at neutral pH limits its use as photosensitizer.

Our previous work in this area has also focused on synthesis of  $[(bpy)_2RuL'_{DQ}]^{4+}$  ( $L' = 1,4$ -bis[2-(4'-methyl)-2,2'-bipyrid-4-yl]-ethenyl]benzene) in solution and attached to a zeolite surface,

\* To whom correspondence should be addressed. E-mail: dutta.1@osu.edu. Phone: 614-292-4532. Fax: 614-688-5402.

along with steady-state photochemistry and electron transfer to bipyridinium ions within the zeolite.<sup>15</sup> We have also studied [(bpy)<sub>2</sub>RuL<sub>DQ</sub>]<sup>4+</sup> (bpy = bipyridine, L<sub>DQ</sub> = 1-[4-(4'-methyl)-2,2'-bipyridyl]-2-[4-(4'-N,N'-tetramethylene-2,2'-bipyridinium)]ethene) attached to a zeolite membrane surface and noticed electron migration within the membrane upon steady-state light illumination.<sup>16</sup> The steady-state photolysis experiments led to higher yields of the viologen radicals in the case of [(bpy)<sub>2</sub>RuL<sub>DQ</sub>]<sup>4+</sup>/zeolite as compared to [(bpy)<sub>2</sub>RuL'<sub>DQ</sub>]<sup>4+</sup>/zeolite.

In this study, we have focused on the synthesis and isolation of [(bpy)<sub>2</sub>RuL<sub>DQ</sub>]<sup>4+</sup> and contrast its solution-based photochemistry with zeolite-based photochemistry, including transient spectroscopic studies. We have also synthesized [(bpy)<sub>2</sub>RuL]<sup>2+</sup> and use it as a model system to understand the chemistry of [(bpy)<sub>2</sub>RuL<sub>DQ</sub>]<sup>4+</sup>. Mass spectroscopy of [(bpy)<sub>2</sub>RuL]<sup>2+</sup> and [(bpy)<sub>2</sub>RuL<sub>DQ</sub>]<sup>4+</sup> are presented. The electrochemical and photophysical properties are also examined. These photosensitizers were incorporated into the nanometer-sized zeolite Y and the photoinduced electron transfer to intrazeolitic viologens studied by transient diffuse reflectance spectroscopy.

## Experimental Section

**Materials and Reagents.** The reagents SeO<sub>2</sub> (Aldrich), 4,4'-dimethyl-2,2'-bipyridine (dmb, Aldrich), 1,4-dibromobutane (Aldrich), trifluoromethanesulfonic anhydride (Aldrich), Ru(bpy)<sub>3</sub>Cl<sub>2</sub> (Strem chemicals), and (bpy)<sub>2</sub>RuCl<sub>2</sub>·2H<sub>2</sub>O (Strem chemicals) were used as received. Tetrahydrofuran (THF), acetonitrile, ethanol, toluene, and *n*-hexane were dried and distilled before use. [Ru(bpy)<sub>3</sub>](PF<sub>6</sub>)<sub>2</sub> was prepared by treating a solution of the Cl<sup>-</sup> salt with saturated NH<sub>4</sub>PF<sub>6</sub> (or KPF<sub>6</sub>) solution. The resulting powdery red precipitate was collected by filtration.

The reagents used for preparing the zeolite synthesis solution were Ludox SM-30 colloidal (30 wt % suspension in water) from Aldrich, tetramethylammonium hydroxide (25 wt % aqueous solution) from Sachem, Inc., aluminum hydroxide (80.5%) from Alfa Aesar, and distilled water. Other materials used were sodium hydroxide from Mallinckrodt and DOWEX HCR-S ion-exchange resin (20–50 dry mesh) from Aldrich for pH adjustment. Methylviologen (MV<sup>2+</sup>, Aldrich) was purified by crystallization from methanol/acetone.

**Instrumentation. Nuclear Magnetic Resonance (NMR) Spectroscopy.** All NMR spectra were acquired on a Bruker DPX400 MHz spectrometer.

**UV–Vis Spectroscopy.** The UV–vis absorption spectra of the ruthenium complexes were measured on a Shimadzu UV-2501PC UV–vis spectrophotometer. Diffuse reflectance spectra of zeolite samples were recorded using an integrating sphere attachment, with zeolite Y as the reference.

**Emission Spectroscopy.** Emission spectra were recorded using a SPEX Fluorolog fluorimeter. The samples were purged with nitrogen gas and excited at 450 nm. Emission quantum yields were measured using [Ru(bpy)<sub>3</sub>]<sup>2+</sup> in oxygen-free acetonitrile (Φ = 0.062) as the reference.

**Transient Absorption.** Time-resolved diffuse reflectance (TRDR) spectra of [(bpy)<sub>2</sub>RuL<sub>DQ</sub>]<sup>4+</sup>-MV<sup>2+</sup>/zeolite Y were measured using a Nd:YAG Q-switched laser (Continuum Surelite with OPO). The pulsed laser source had a temporal width of 15 ns with a pulse power of 21–24 mW and operated at a frequency of 1 Hz. A pulsed xenon lamp (150 W, Applied Photophysics) was used as the probe, and the diffusely reflected light was collected and focused into a spectrometer (150 g/mm grating, SPEX 1877 Triplemate). Two detection systems were used. A photodiode array (EG &G Princeton Applied Research),

with timing of the laser pulse, lamp pulse, time delay, and detection window (100 ns) being controlled with an EG&G high-voltage pulse generator and a National Instrument PCI 6602 Card for triggering the Q-switch and lamp pulse. The second detection system was an Andor iStar (DH 734) ICCD camera. The zeolite suspension was sealed in a 1 mm cell and purged with argon or nitrogen continuously. The sample was excited at 458 nm, and the TRDR spectra were acquired at ~100 ns after sample excitation and at a various time delays up to 1 ms. Each spectrum was an average of 100 shots.

**Electrospray Ionization Mass Spectrometry (ESI-MS).** The experiments were performed on a Micromass ESI-ToF II (Micromass, Wythenshawe, UK) mass spectrometer equipped with an orthogonal electrospray source (Z-spray) operated in positive ion mode. Sodium iodide was used for mass calibration for a calibration range of *m/z* 100–2000. Samples were prepared in a solution containing acidified methanol and infused into the electrospray source at a rate of 5–10 mL min<sup>-1</sup>. For exact mass measurements, the spectra were combined, smoothed and centroided, and internal calibration with sodium iodide clusters was used. Optimal ESI conditions were: capillary voltage 3000 V, source temperature 110 °C, and a cone voltage of 55 V. The ESI gas was nitrogen.

**Electrochemistry.** Electrochemistry measurements were carried out with a Princeton Applied Research model 273 potentiostat, using a conventional three-electrode cell assembly. A freshly polished platinum disk electrode (2 mm diameter, CHI Instruments) as working electrode, a platinum wire electrode as counter electrode, and Ag/AgCl reference electrode were used. Potentials are quoted versus the ferrocene–ferrocenium (Fc/Fc<sup>+</sup>) couple since ferrocene was used as an internal standard. Acetonitrile was used as solvent, and 0.10 M tetrabutylammonium hexafluorophosphate (TBAPF<sub>6</sub>) was used as supporting electrolyte.

**X-ray Powder Diffraction (XRD).** The XRD patterns were recorded with a Rigaku Geigerflex diffractometer using Ni-filtered Cu Kα radiation (40 kV and 25 mA).

**Scanning Electron Microscopy.** Particle morphologies were obtained using a JEOL 820 scanning electron microscope. The crystal sizes were measured from TEM images.

**Kinetic Modeling.** The BET kinetics were modeled using a system dynamics modeling software, STELLA, provided by High Performance Systems, Inc. The software uses the Runge–Kutta Methods for numerical simulation. The simulation results were visually compared with the experimental data for obtaining the best fits.<sup>10</sup>

**Synthesis of Ruthenium Complexes. Synthesis of [(bpy)<sub>2</sub>RuL]<sup>2+</sup>.** Ligand L (**1a**) was synthesized according to the literature.<sup>12</sup> <sup>1</sup>H NMR (400 MHz, CDCl<sub>3</sub>): δ 8.72 (d, 2H), 8.67 (s, 2H), 8.61 (d, 2H), 8.32 (s, 2H), 7.52 (s, 2H), 7.45 (d, 2H), 7.21 (d, 2H), 2.49 (s, 6H). [(bpy)<sub>2</sub>RuL]<sup>2+</sup> (**1b**) was synthesized as described in Scheme S1 (Supporting Information). Ligand L (100 mg, 0.27 mmol) was dissolved in 30 mL of EtOH–H<sub>2</sub>O (3:1, v/v), and [(bpy)<sub>2</sub>RuCl<sub>2</sub>·H<sub>2</sub>O] (0.044 g, 0.09 mmol) was added and refluxed overnight. The product was precipitated with an aqueous solution of KPF<sub>6</sub> and purified by column chromatography on neutral alumina (grade III) using acetonitrile/toluene mixtures (6:4, v/v) as eluent. <sup>1</sup>H NMR (400 MHz, CD<sub>2</sub>Cl<sub>2</sub>): δ 8.75–7.16 (30H), 2.67 (s, 3H), 2.49 (s, 3H). ESI-MS (*m/z*): 923.1 [M – PF<sub>6</sub><sup>-</sup>]<sup>+</sup>, 389.1 [M – 2PF<sub>6</sub><sup>-</sup>]<sup>2+</sup>, 311.1 [M – (bpy) – 2PF<sub>6</sub><sup>-</sup>]<sup>2+</sup>. The chloride salt [(bpy)<sub>2</sub>RuL]Cl<sub>2</sub> was prepared by treating a solution of the PF<sub>6</sub><sup>-</sup> salt in acetone with lithium chloride.

**Synthesis of [(bpy)<sub>2</sub>RuL<sub>DQ</sub>]<sup>4+</sup>.** The synthesis of the [(bpy)<sub>2</sub>RuL<sub>DQ</sub>]<sup>4+</sup> (**1d**) complex was accomplished in three steps, as depicted in Scheme S1 (Supporting Information). 1,4-Butane dinitrile was prepared according to the literature.<sup>17</sup> A solution of 1.08 g (0.015 mol) of THF in CH<sub>2</sub>Cl<sub>2</sub> (50 mL) was added dropwise to a solution of 4.95 g (0.015 mol) of trifluoromethanesulfonic anhydride in CH<sub>2</sub>Cl<sub>2</sub> (50 mL) at -78 °C. The reaction mixture was allowed to warm to ambient temperature and then extracted. Evaporation and recrystallization of the residue from CH<sub>2</sub>Cl<sub>2</sub> gave a yield of 2.8 g (53%). <sup>1</sup>H NMR (400 MHz, CDCl<sub>3</sub>), δ 4.63 (m, 4 H), 2.03 (m, 4 H).

L<sub>DQ</sub>(OTf)<sub>2</sub> (**1c**) was prepared by stirring a solution of ligand L (**1a**) (0.5 g, 3.20 mmol) and 1,4-butane dinitrile (1.1 g, 3.37 mmol) in dichloromethane at room temperature for 3 days. The mixture was evaporated to dryness and the residue suspended in CHCl<sub>3</sub>. Filtration of the suspension yielded a white powder, which was dried in vacuo. The final yield was 1.32 g (85%) of base on L ligand. <sup>1</sup>H NMR (400 MHz, CDCl<sub>3</sub>): δ 8.96 (d, 1H), 8.90 (d, 1H), 8.78 (d, 1H), 8.69 (s, 1H), 8.55 (d, 1H), 8.44 (dd, 1H), 8.40 (s, 1H), 8.31 (s, 1H), 8.20 (d, 1H), 8.12 (s, 1H), 8.03 (d, 1H, *J* = 16 Hz), 7.78 (d, 1H, *J* = 16 Hz), 7.67 (dd, 1H), 7.29 (dd, 1H), 4.73 (m, 2H), 4.07 (m, 2H), 2.78 (s, 3H), 2.47 (s, 3H), 2.38 (t, 2H), 2.08 (t, 2H). ESI-MS (*m/z*): 569.1 [M - OTf]<sup>+</sup>, 210.1 [M - 2OTf]<sup>2+</sup>.

L<sub>DQ</sub>(OTf)<sub>2</sub> (**1c**) (300 mg, 0.42 mmol) was dissolved in 150 mL of a water/ethanol mixture (1:1, v/v) and [(bpy)<sub>2</sub>RuCl<sub>2</sub>·2H<sub>2</sub>O] (250 mg, 0.48 mmol) was added and refluxed for 24 h. The resulting solution was reduced to ~50 mL and filtered. Saturated NH<sub>4</sub>PF<sub>6</sub> aqueous solution was added to yield a crude solid product as the PF<sub>6</sub><sup>-</sup> salt. The product was purified by column chromatography on grade 60, 230–400 mesh silica gel, eluting with a solvent mixture of acetonitrile/distilled water/saturated aqueous KNO<sub>3</sub>. The elution was started with a ratio of 2:6:2 and slowly changed to 5:4:1. The fraction containing the desired product was collected, and the solvent was removed under reduced pressure. <sup>1</sup>H NMR (400 MHz, CD<sub>2</sub>Cl<sub>2</sub>): δ 9.0–7.26 (30H), 4.74 (m, 2H), 4.10 (m, 2H), 2.78 (s, 3H), 2.58 (s, 3H), 2.39 (m, 2H), 2.10 (m, 2H). ESI-MS (*m/z*): 416.6 [M - H<sup>+</sup> - 4PF<sub>6</sub>]<sup>2+</sup>, 480.6 [M - 4PF<sub>6</sub> - I]<sup>2+</sup>, 489.6 [M - 3PF<sub>6</sub>]<sup>2+</sup>. The chloride salt was prepared by treating a solution of the PF<sub>6</sub><sup>-</sup> salt in acetone with lithium chloride.

**Synthesis of Zeolite Composites. Nanocrystalline Zeolite Y.** Nanocrystalline zeolite Y was synthesized from clear homogeneous solutions with a molar composition of 3.13 (TMA)<sub>2</sub>O:0.0016 Na<sub>2</sub>O:1.0 Al<sub>2</sub>O<sub>3</sub>:4.32 SiO<sub>2</sub>:497 H<sub>2</sub>O.<sup>9</sup> A Ludox silica solution (30.2 wt % SiO<sub>2</sub>, 0.66 wt % Na<sub>2</sub>O) was adjusted to a pH of 8.1 (reduce Na<sup>+</sup>) with a cationic ion-exchange resin, DOWEX HCR-S (H<sup>+</sup> form). Tetramethylammonium hydroxide (53.6 g) was added to an aqueous solution (152 mL H<sub>2</sub>O) of aluminum hydroxide (4.58 g) and stirred for 2 h to give a clear solution. A small amount of sodium hydroxide was added to the solution and stirred for 30 min. Then silica solution (20 g) was slowly added with constant vigorous stirring, and the resulting solution was further stirred for about 2 h. For carrying out the zeolite crystallization, the solutions were transferred to a flask containing a magnetic stirrer and heated at 90 °C in a preheated oil bath. The synthesis process was monitored visually. The clear synthesis solution gradually became cloudier. After isolating the nanocrystals, the remaining clear solution (mother liquor) was returned to the flask and the same amount of NaOH as in the original synthesis solution was added to the mother liquor for the next synthesis batch. The process was repeated and lasted ~30 days to yield 903 mg of zeolite. All samples were centrifuged using a high-speed ultracentrifuge at

24000 rpm to remove the solid material, which was then washed and dried in a vacuum oven at 60 °C.

**MV<sup>2+</sup>/Zeolite.** Methylviologen (MV<sup>2+</sup>) was incorporated into zeolite Y by ion-exchange. In a typical experiment, 1.0 g of zeolite was mixed with 95 mg of MV<sup>2+</sup> (37 mM) in 10 mL of deionized water, and the mixture was stirred for 24 h at room temperature. The sample was washed thoroughly with deionized water, collected by ultracentrifuge, and dried at 40 °C. To reach maximum loading level, the ion-exchange experiment was repeated twice.

**[(bpy)<sub>2</sub>RuLH]<sup>3+</sup>/Zeolite Y.** Attachment of [(bpy)<sub>2</sub>RuL]<sup>2+</sup> on zeolite was achieved by ion-exchange. An aqueous solution of [(bpy)<sub>2</sub>RuL]<sup>2+</sup> was adjusted to pH ≈ 4 by adding HCl. A colloidal solution of zeolite was added and stirred overnight. Then the sample was washed with pH 4 aqueous solution and followed by distilled water. The orange-colored solid was collected by ultracentrifuge and dried at 40 °C.

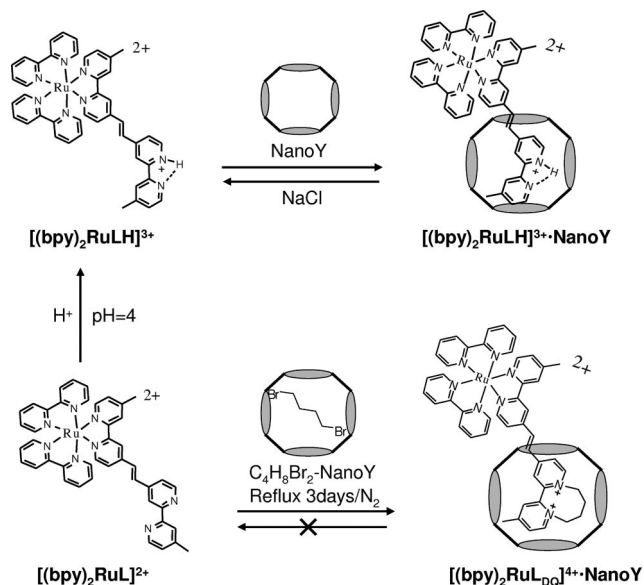
**[(bpy)<sub>2</sub>RuL<sub>DQ</sub>]<sup>4+</sup>/Zeolite Y.** [(bpy)<sub>2</sub>RuL<sub>DQ</sub>]<sup>4+</sup> photosensitizer was permanently anchored on the surface of zeolite by a ship-in-bottle strategy. The as-synthesized zeolite was calcined at 500 °C for 6 h under a flow of air. Then the sample was ion-exchanged with 1.0 M NaCl solution for 24 h. Zeolite (1.0 g) was transferred to a quartz tube and heated under high vacuum (>10<sup>4</sup> Torr) at 80 °C, the activated sample was transferred to a nitrogen-filled glovebox, and 15 mL of dried *n*-hexane was added. 1,4-Dibromobutane (C<sub>4</sub>H<sub>8</sub>Br<sub>2</sub>, 0.12 mL) was then added to the zeolite suspension and stirred under nitrogen for 24 h. [(bpy)<sub>2</sub>RuL]<sup>2+</sup> (23 mg, 25 μmol) and C<sub>4</sub>H<sub>8</sub>Br<sub>2</sub>/zeolite (0.5 g) were mixed in 16 mL of CH<sub>3</sub>CN/toluene (dried, 3:1), and refluxed for 3 days. The product was washed by acetonitrile to remove any surface species. The excess dibromobutane was Soxhlet-extracted with chloroform until it was no longer found in the solvent (typically 2–3 weeks) as measured by UV–visible spectroscopy. The resulting pink-red solid was washed thoroughly with 0.5 M NaCl at room temperature followed by sonication at 55 °C with 0.5 M NaCl to remove any Ru(II) complex not encapsulated in the zeolite surface. Finally, the solid was washed with distilled water to remove NaCl.

**[(bpy)<sub>2</sub>RuL<sub>DQ</sub>]<sup>4+</sup>/MV<sup>2+</sup>/Zeolite Y.** Incorporation of MV<sup>2+</sup> was achieved by ion-exchange.

## Results

**Synthesis of [(bpy)<sub>2</sub>RuL]<sup>2+</sup> (**1b**) and [(bpy)<sub>2</sub>RuL<sub>DQ</sub>]<sup>4+</sup> (**1d**) Complexes.** Ligand L (**1a**) was prepared by the method of Strouse et al.<sup>12</sup> The <sup>1</sup>H NMR spectrum of the product is consistent with the formation of the trans isomer. Compound [(bpy)<sub>2</sub>RuL]<sup>2+</sup> (**1b**) was synthesized by reaction of [(bpy)<sub>2</sub>RuCl<sub>2</sub>] with ligand L (synthetic scheme shown in Supporting Information, Scheme S1). The <sup>1</sup>H NMR spectrum exhibits chemical shifts at ~7.5 (7.50, 7.54, d, 1 H, *J* = 16 Hz) and 7.65 ppm (7.60, 7.64, d, 1 H, *J* = 16 Hz), which are assigned to the olefinic protons (Supporting Information, Figure S1). The large coupling constant indicates the formation of the trans isomer.

Diquats (DQs) are usually prepared as bromide salts by refluxing the appropriate α-diimine with dibromoalkane.<sup>18,19</sup> Elliott et al. have synthesized bridged diquaternary salts in which the nitrogens of the DQ were connected by a chain of methylene groups of length *n* (*n* = number of carbons, *n* = 2, 3, 4).<sup>20–22</sup> Synthesis of compound [(bpy)<sub>2</sub>RuL<sub>DQ</sub>]<sup>4+</sup> (**1d**) was attempted by direct quaternization of bipyridine end of **1b** with X(CH<sub>2</sub>)<sub>4</sub>X (X = Br, I, and triflate); these reactions were unsuccessful. The alternative strategy for preparation of **1d** involved quaternization of the bipyridine end of L ligand. Reactions of **1a** with 1,4-dibromobutane and 1,4-diiodobutane resulted in low yields of

**SCHEME 1: Schematic of Attachment of [(bpy)<sub>2</sub>RuL]<sup>2+</sup> and [(bpy)<sub>2</sub>RuL<sub>DQ</sub>]<sup>4+</sup> on a Surface of Zeolite Y**


the quaternized compound. In contrast, when triflate was used as a leaving group,<sup>17,23</sup> the reaction could be carried out at room temperature and the yield was high (85%). The structure of **1c** was confirmed by <sup>1</sup>H NMR (Supporting Information, Figure S2) and mass spectrometry. Chemical shifts of the aromatic protons and methyl protons of **1c** are split as compared to **1a**, since the symmetry of **1a** is destroyed due to quaternization of the bipyridine end. The large coupling constant between the two olefinic protons [ $\delta$  8.03 (d, 1 H,  $J = 16$  Hz); 7.78 (d, 1 H,  $J = 16$  Hz)] indicates that the product is solely the trans isomer. This result is consistent with the fact that starting reagent **1a** is the trans isomer. The peaks with chemical shifts at  $\sim 4.7$  (2H),  $\sim 4.1$  (2H),  $\sim 2.4$  (2H),  $\sim 2.1$  ppm (2H) (which overlaps with the solvent residue peak at  $\sim 2.2$  ppm) are assigned to the alkyl protons (8H) of the DQ ring.

Compound **1d** was synthesized by refluxing [(bpy)<sub>2</sub>RuCl<sub>2</sub>] with L<sub>DQ</sub> ligand (**1c**) in a mixture of EtOH/H<sub>2</sub>O (1:1) for 24 h. The <sup>1</sup>H NMR spectrum (Supporting Information, Figure S3) exhibited chemical shifts at  $\sim 4.8$  (2H),  $\sim 4.10$  (2H),  $\sim 2.4$  (2H),  $\sim 2.1$  ppm (2H, buried under solvent residue peaks) and attributed to the alkyl protons (8H) of DQ moiety. A large coupling constant ( $J = 16$  Hz) between two olefinic protons [ $\delta$  7.95 (7.90, 7.95, d, 1H,  $J = 16$  Hz); 7.85 (7.80, 7.85, d, 1H,  $J = 16$  Hz)] indicates that L<sub>DQ</sub> maintains its trans geometry. The chemical shifts of the aromatic protons of L<sub>DQ</sub> (7–9 ppm) in [(bpy)<sub>2</sub>RuL<sub>DQ</sub>]<sup>4+</sup> are shifted to lower field compared to those of [(bpy)<sub>2</sub>RuL]<sup>2+</sup> due to the positive charge of the quaternary nitrogens.

The synthetic strategies for attachment of [(bpy)<sub>2</sub>RuL]<sup>2+</sup> and [(bpy)<sub>2</sub>RuL<sub>DQ</sub>]<sup>4+</sup> on surface of zeolite Y are shown in Scheme 1. For [(bpy)<sub>2</sub>RuL]<sup>2+</sup>, the monoprotonated complex was made by adjusting the pH to 4, and this species was surface ion-exchanged onto the zeolite in a pH 4 solution. For [(bpy)<sub>2</sub>RuL<sub>DQ</sub>]<sup>4+</sup> incorporation into the zeolite, the zeolite was dehydrated and its cages filled with 1,4-dibromobutane, [(bpy)<sub>2</sub>RuL]<sup>2+</sup> was then adsorbed onto the zeolite and the solid mixture heated under reflux for 72 h. This was followed by extensive ion-exchange to remove surface bound Ru species. Internal quaternization of the [(bpy)<sub>2</sub>RuL<sub>DQ</sub>]<sup>4+</sup> as shown in Scheme 1 entraps part of L<sub>DQ</sub> in the zeolite supercage and cannot be removed by ion-exchange, whereas, [(bpy)<sub>2</sub>RuLH]<sup>3+</sup> held

**TABLE 1: Reduction Potentials for Ruthenium Complexes<sup>a</sup>**

compounds	E <sub>1/2</sub> , V					
	Ru <sup>3+/2+</sup>	DQ <sup>2+/+</sup>	DQ <sup>+0</sup>	Ru <sup>2+/+</sup>	Ru <sup>+0</sup>	Ru <sup>0/-</sup>
[Ru(bpy) <sub>3</sub> ] <sup>2+</sup>	0.89			-1.74	-1.93	-2.18
[Ru(bpy) <sub>2</sub> L] <sup>2+</sup>	0.91			-1.65	-1.86	-2.13
[Ru(bpy) <sub>2</sub> L <sub>DQ</sub> ] <sup>4+</sup>	0.91	-0.90	-1.32	-1.77	-1.92	

<sup>a</sup> As PF<sub>6</sub><sup>-</sup> salts. All potentials are versus Fc<sup>+/0</sup> in CH<sub>3</sub>CN solution with 0.1 M TBAPF<sub>6</sub> as supporting electrolyte  $\nu = 100$  mV s<sup>-1</sup>.

by electrostatic force is ion-exchangeable. In solution, quaternization with 1,4-dihaloalkanes led to very low yields due to the second-order reaction, but in the zeolite, the supercage brings the reactants in intimate contact and promotes this second-order reaction. The Ru loading of [(bpy)<sub>2</sub>RuL<sub>DQ</sub>]<sup>4+</sup> was determined to be 5.1  $\mu$ mol g<sup>-1</sup> zeolite by ICP-OES (Galbraith Laboratories).

**Mass Spectrometry of [(bpy)<sub>2</sub>RuL]<sup>2+</sup> and [(bpy)<sub>2</sub>RuL<sub>DQ</sub>]<sup>4+</sup> Complexes.** The mass spectra (electrospray ionization) of [(bpy)<sub>2</sub>RuL](PF<sub>6</sub>)<sub>2</sub> and [(bpy)<sub>2</sub>RuL<sub>DQ</sub>](PF<sub>6</sub>)<sub>4</sub> are shown in Supporting Information, Figure S4. The most abundant ion of [(bpy)<sub>2</sub>RuL](PF<sub>6</sub>)<sub>2</sub> was found at  $m/z = 389.1051$  and assigned to [M - 2(PF<sub>6</sub><sup>-</sup>)]<sup>2+</sup> (calculated composition [RuC<sub>44</sub>H<sub>36</sub>N<sub>8</sub>]<sup>2+</sup>; exact mass = 389.1054). The ion centered at  $m/z = 923.1$  corresponds to the singly charged [M - (PF<sub>6</sub><sup>-</sup>)]<sup>+</sup> ion. The mass spectrum of [(bpy)<sub>2</sub>RuL<sub>DQ</sub>](PF<sub>6</sub>)<sub>4</sub> is shown in Supporting Information, Figure S4. The most abundant ion is found at  $m/z = 416.6331$  and corresponds to the calculated composition of [RuC<sub>48</sub>H<sub>43</sub>N<sub>8</sub>]<sup>2+</sup> (exact mass = 416.6328), and assigned to [M - 4(PF<sub>6</sub><sup>-</sup>) - H<sup>+</sup>]<sup>2+</sup>. The doubly charged ions of  $m/z = 480.6$  and 489.6 are assigned to [M - 4(PF<sub>6</sub><sup>-</sup>) + I<sup>-</sup>]<sup>2+</sup> and [M - 3(PF<sub>6</sub><sup>-</sup>)]<sup>2+</sup>, respectively. The source of iodide is from sodium iodide added as an internal standard. The loss of bpy ligand was not observed in either case. These mass spectra of [(bpy)<sub>2</sub>RuL]<sup>2+</sup> and [(bpy)<sub>2</sub>RuL<sub>DQ</sub>]<sup>4+</sup> are best interpreted by invoking two fragmentation channels: (1) the loss of PF<sub>6</sub><sup>-</sup> and (2) the loss of HPF<sub>6</sub> (Supporting Information, Figure S5). Proton loss from a 2,2'-bipyridine complex by dissociation of HCl has been reported.<sup>24</sup> Pyridines upon coordination to highly charged centers as in Cp<sub>2</sub>Zr<sup>IV</sup>(py)<sub>2</sub> are reported to undergo rearrangements with loss of an ortho CH proton.<sup>25</sup>

**Electrochemistry.** Electrochemical properties of the ruthenium complexes were studied by cyclic voltammetry (CV), and the data are summarized in Table 1. Ferrocene was used as an internal standard. In the CV of [Ru(bpy)<sub>2</sub>L]<sup>2+</sup> (Figure 1a), the redox couple at 0.91 V (vs ferrocene) is due to the Ru<sup>(III/II)</sup>-based redox process. Three ligand-localized reductions appear at -1.65, -1.86, and -2.13 V. The redox couple at -1.65 V is assigned to the [L/L<sup>-</sup>] redox couple. The other two reductions are from bpy ligands. The cyclic voltammogram of [Ru(bpy)<sub>2</sub>L<sub>DQ</sub>]<sup>4+</sup> shows one oxidation wave at 0.91 V due to Ru<sup>(III/II)</sup> and four ligand-based reduction waves at -0.90, -1.32, -1.77, and -1.92 V, as shown in Figure 1b. The redox waves at -0.90 and -1.32 V are assigned to the reduction of the DQ part of the ligand [(DQ)<sup>2+/+</sup>/(DQ)<sup>+0</sup>] and [(DQ)<sup>+0</sup>/(DQ)<sup>0</sup>], respectively. The CV of [Ru(bpy)<sub>2</sub>L<sub>DQ</sub>]<sup>4+</sup> was broad and quasi-reversible, especially at low scan rates. This is due to the tendency of the olefinic ligand to form polymeric films on the working Pt electrode due to reductive electropolymerization, a process that has been observed for diimine complexes with olefinic moieties.<sup>13</sup>

**Nanozeolite Synthesis and Characterization.** Use of nanometer-sized zeolite Y offers two potential advantages. First, the small size affords a higher surface area and, thereby, increased surface loading of the sensitizer complexes. Second,

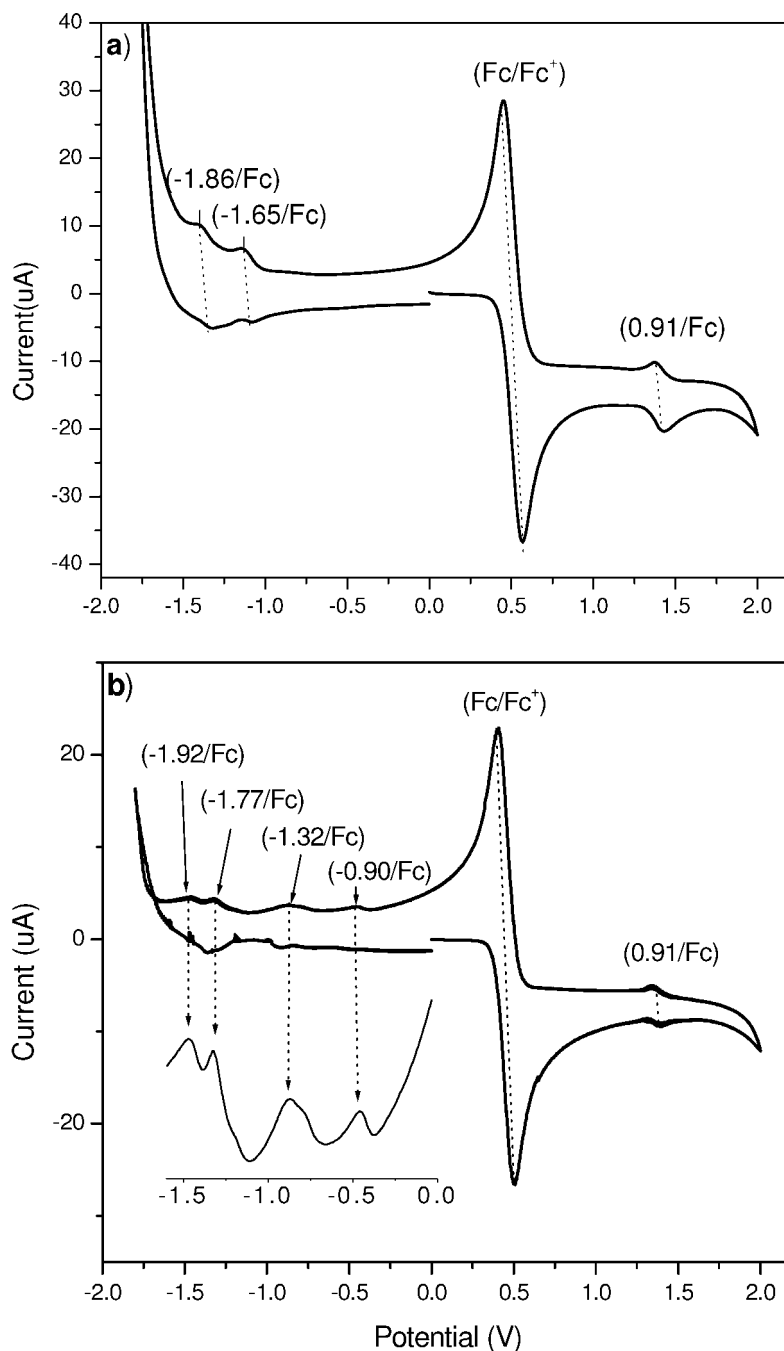


**Figure 1.** Cyclic voltammogram of (a)  $[\text{Ru}(\text{bpy})_2\text{L}](\text{PF}_6)_2$  and (b)  $[\text{Ru}(\text{bpy})_2\text{LDQ}](\text{PF}_6)_4$  in  $\text{CH}_3\text{CN}$  containing ferrocene with 0.1 M  $\text{TBAPF}_6$  as supporting electrolyte,  $\nu = 0.1 \text{ V s}^{-1}$ . Reference electrode is  $\text{Ag}/\text{AgCl}$ .

nanozeolite dispersions are optically transparent, making it possible to use transmission spectroscopic methods to study intrazeolitic species.<sup>9</sup> Crystallization of zeolites from gel systems usually lead to broad particle size distributions (PSDs) because the nucleation and crystal growth processes occur simultaneously. Colloidal zeolites with relatively narrow PSDs have been prepared from homogeneous solutions.<sup>26</sup> Crystallization of zeolite is sensitive to factors such as the alkali concentration, Si/Al ratio, aging time, and hydrothermal treatment.<sup>27,28</sup> To reduce the formation of zeolite A, the initial sodium ion concentration was kept low and during the synthesis, equal portions of  $\text{Na}^+$  was added at regular intervals. The zeolite formed was recovered prior to addition of  $\text{Na}^+$  and the synthesis continued. By repeated use of mother liquor, zeolite yield was increased with zeolite

Y as the sole final product. Figure 2a shows the XRD powder pattern and is consistent with pure phase zeolite Y. Figure 2b shows the TEM image of the zeolite crystallites, with average particle sizes of  $\sim 80 \text{ nm}$ .

**Spectroscopy of  $[(\text{bpy})_2\text{RuL}]^{2+}$  and  $[(\text{bpy})_2\text{RuLDQ}]^{4+}$  in Solution and Zeolite.** The absorption spectra of  $[(\text{bpy})_2\text{RuL}]^{2+}$ , monoprotonated  $[(\text{bpy})_2\text{RuLH}]^{3+}$ , and  $[(\text{bpy})_2\text{RuLDQ}]^{4+}$  in solution are compared in Figure 3a. These complexes have an absorption band at  $\sim 287 \text{ nm}$ , assigned to intraligand  $\pi-\pi^*$  transitions of bpy. The absorption band at  $\sim 330 \text{ nm}$  is attributed to intraligand  $\pi-\pi^*$  transitions of ligand L,  $\text{LH}^+$ , and  $\text{LDQ}$ . Upon monoprotonation, the intensity of the 330 nm band increases, and further so in the case of  $[(\text{bpy})_2\text{RuLDQ}]^{4+}$ . MLCT transitions for  $[(\text{bpy})_2\text{RuL}]^{2+}$ , monoprotonated  $[(\text{bpy})_2\text{RuLH}]^{3+}$  appear at  $\sim 460 \text{ nm}$ , for  $[(\text{bpy})_2\text{RuLDQ}]^{4+}$  the band is red-shifted to  $\sim 500$

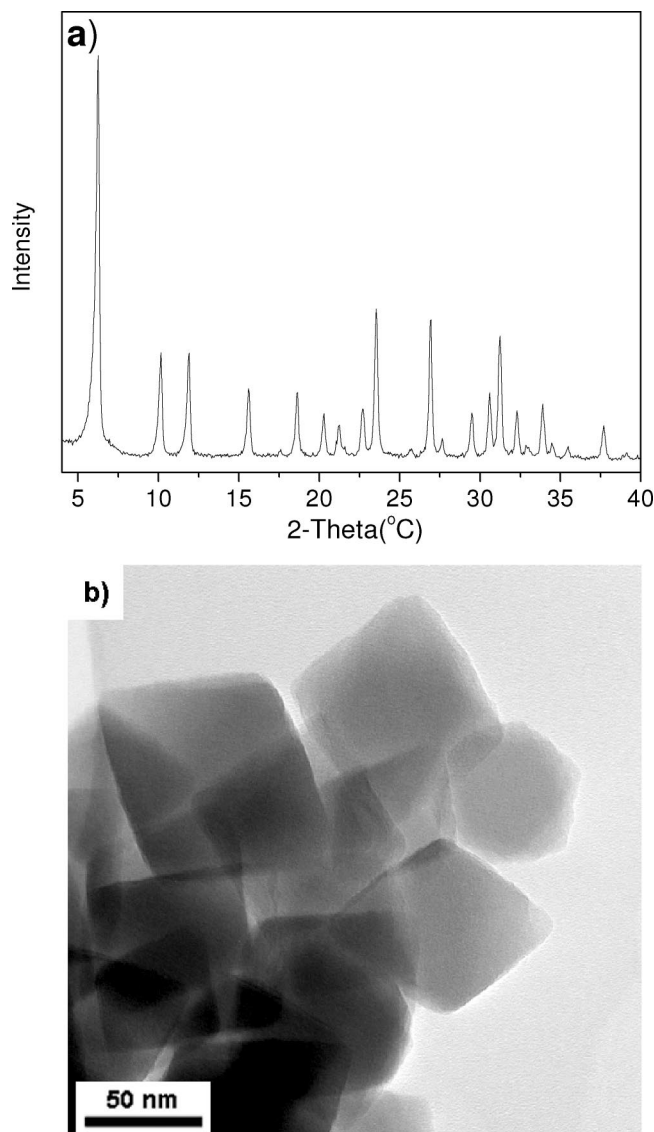


**Figure 2.** (a) Powder diffraction pattern of nanocrystalline zeolites; (b) TEM image of nanocrystalline zeolites.

nm. The inset of Figure 3a compares the absorption spectra of  $[(bpy)_2RuL_{DQ}]^{4+}$  and diprotonated (both N's of L are protonated)  $[(bpy)_2RuLH_2]^{4+}$ . Both these complexes have similar spectral patterns and are a reflection of the quaternization of both the bpy nitrogens in L. These results are consistent with previous studies that MLCT bands exhibit red-shifts when nitrogen atoms on pendant pyridyl ligands are protonated or methylated.<sup>29</sup>

Absorption measurements of nanozeolite suspensions of  $[(bpy)_2RuLH]^{3+}/Y$  and  $[(bpy)_2RuL_{DQ}]^{4+}/Y$  were carried out in transmission mode and the results are shown in Figure 3b. The intraligand  $\pi-\pi^*$  transition of  $L_{DQ}$ , indicating the presence of  $-C=C-$  bond and the MLCT bands are observed.

Figure 4a shows the emission spectra of the ruthenium polypyridyl complexes in solution. The emission maximum of  $[(bpy)_2RuL]^{2+}$  is at  $\sim 675$  nm and a quantum yield one-tenth of that of  $[Ru(bpy)_3]^{2+}$  (emission maximum  $\sim 620$  nm). The decrease in the quantum yield of  $[(bpy)_2RuLH]^{3+}$  upon protonation was noted earlier.<sup>14</sup> The emission of  $[(bpy)_2RuL_{DQ}]^{4+}$  is very weak, and for all practical purposes can be considered quenched. Figure 4b shows the emission spectra of  $[(bpy)_2RuLH]^{3+}$  and  $[(bpy)_2RuL_{DQ}]^{4+}$  in zeolite. A  $\sim 30$  nm red-shift of emission  $\lambda_{max}$  of  $[(bpy)_2RuLH]^{3+}$  is observed. Though no

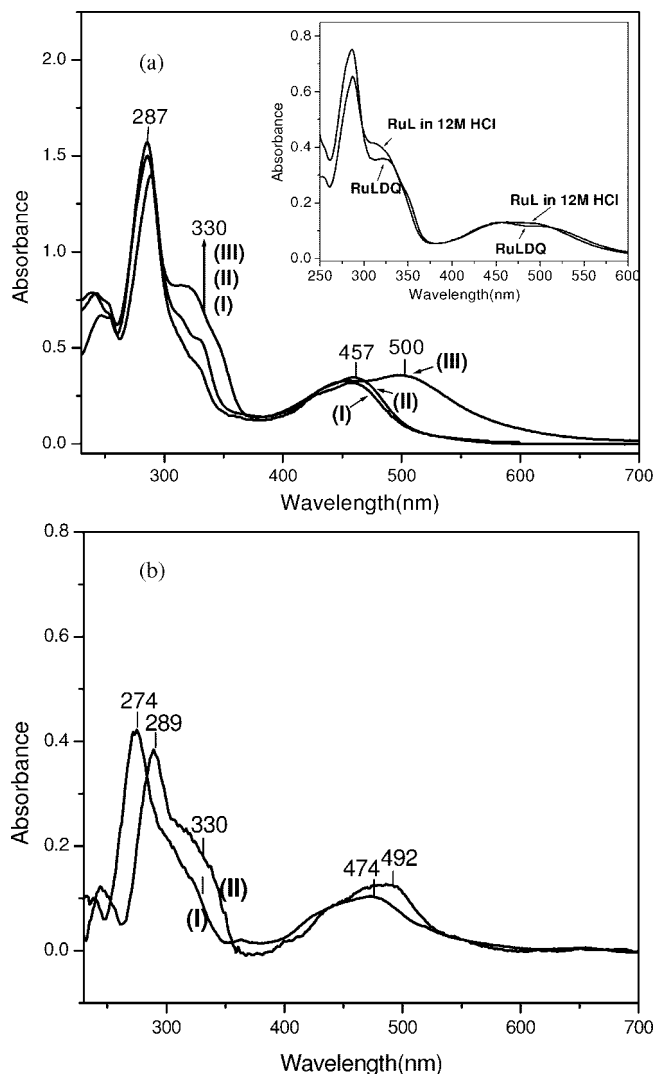


**Figure 3.** (a) Absorption spectra of  $[(bpy)_2RuL]^{2+}$  (I),  $[(bpy)_2RuLH]^{3+}$  (II), and  $[(bpy)_2RuL_{DQ}]^{4+}$  (III) in  $CD_3CN$ . Inset shows absorption spectra of  $[(bpy)_2RuL_{DQ}]^{4+}$  in water and  $[(bpy)_2RuL]^{2+}$  in 12 M HCl. (b) Absorption spectra of  $[(bpy)_2RuLH]^{3+}$  (I) and  $[(bpy)_2RuL_{DQ}]^{4+}$  (II) on zeolites (data taken in transmission mode, baseline corrected).

emission of  $[(bpy)_2RuL_{DQ}]^{4+}$  was observed in solution, upon attachment to the zeolite, a band appears at  $\sim 695$  nm.

The excited-state decay for  $[(bpy)_2RuL]^{2+}$  in  $CH_3CN$  was fit with a biexponential fit of 710 (82%) and 256 (18%) ns.<sup>14</sup> The lifetime of  $[(bpy)_2RuL_{DQ}]^{4+}$  in solution was not observable on the nsec measurement system. However, upon incorporation in the zeolite, transient diffuse reflectance spectra could be obtained and the data are shown in Figure 5a. Figure 5b shows the decay of the intensity at 370 nm due to the absorption of the  $[(bpy)_2RuL_{DQ}]^{4+}$  and was fit to a monoexponential function, resulting in a lifetime of 796 ns.

**Steady-State Photolysis of  $[(bpy)_2RuL]^{2+}$  and  $[(bpy)_2RuL_{DQ}]^{4+}$  in Aqueous Solution.** The photostability of the complexes in aqueous solutions was studied. An aqueous solution containing  $[(bpy)_2RuL_{DQ}]^{4+}$  was irradiated by visible light for 8 h. No significant spectroscopic changes were observed by absorption spectroscopy (Figure 6), indicating that the complex is stable under visible light. In contrast, significant spectral changes (inset of Figure 6) attributed to the loss of  $-C=C-$  bond of L ligand under visible light illumination of  $[(bpy)_2RuL]^{2+}$  is observed.<sup>14</sup>

**Photoinduced Electron Transfer with  $MV^{2+}$ .** Electron-transfer reactions between  $[(bpy)_2RuL]^{2+}$  ( $1 \times 10^{-5}$  M) and

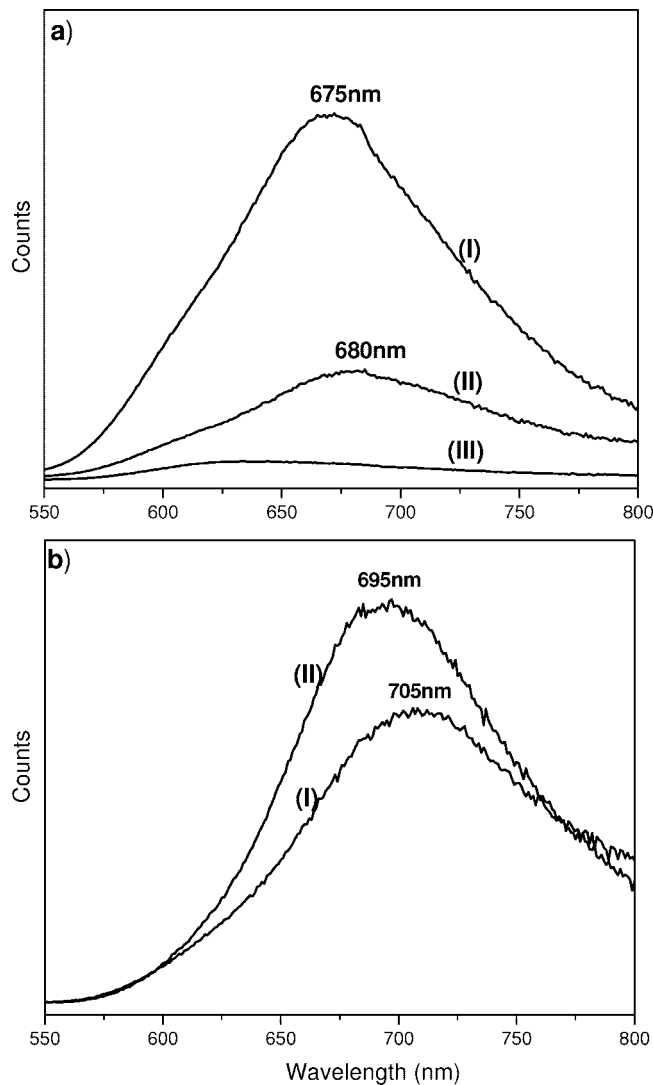


**Figure 4.** (a) Emission spectra of  $[(bpy)_2RuL]^{2+}$  (I),  $[(bpy)_2RuLH]^{3+}$  (II), and  $[(bpy)_2RuLDQ]^{4+}$  (III) in  $CD_3CN$ . (b) Emission spectra of  $[(bpy)_2RuLH]^{3+}$  (I) and  $[(bpy)_2RuLDQ]^{4+}$  (II) on zeolites. (Excitation wavelength = 450 nm).

$MV^{2+}$  in acetonitrile was studied by emission quenching and transient absorption spectroscopy. On the basis of the quenching of the emission shown in Figure 7a, and the corresponding Stern–Volmer plot of Figure 7b, the quenching rate constant  $k_q$  was calculated to be  $4.2 \times 10^8 \text{ L mol}^{-1} \text{ s}^{-1}$ . The time-resolved absorption spectra shown in Figure 7c shows the formation of the  $MV^{+}$  radical, indicating that electron transfer is responsible for the quenching. The electron-transfer reaction between  $[(bpy)_2RuLDQ]^{4+}$  and  $MV^{2+}$  in acetonitrile was also examined by laser flash photolysis, but unlike the  $[(bpy)_2RuL]^{2+}$  system, no evidence of  $MV^{+}$  radical formation was noticed. Even in the presence of a sacrificial electron donor, EDTA (aqueous), no evidence for  $MV^{+}$  was noted.

However, for the  $[(bpy)_2RuLDQ]^{4+}$ /zeolite Y system (dispersion in water), with  $MV^{2+}$  exchanged into the zeolite, emission quenching was noted (inset in Figure 8) and the transient diffuse reflectance spectra show the formation of the  $MV^{+}$  radical, as shown in Figure 8. The signal present at 390 nm following excitation at 458 nm arises from the  $MV^{+}$  radical. Within the first 100 ns (limited by our measurement system), the formation of the  $MV^{+}$  radical is complete. Figure 9 plots the intensity at 390 nm as a function of time (up to 1 ms). There is a rapid decrease in intensity over the first microsecond followed by a

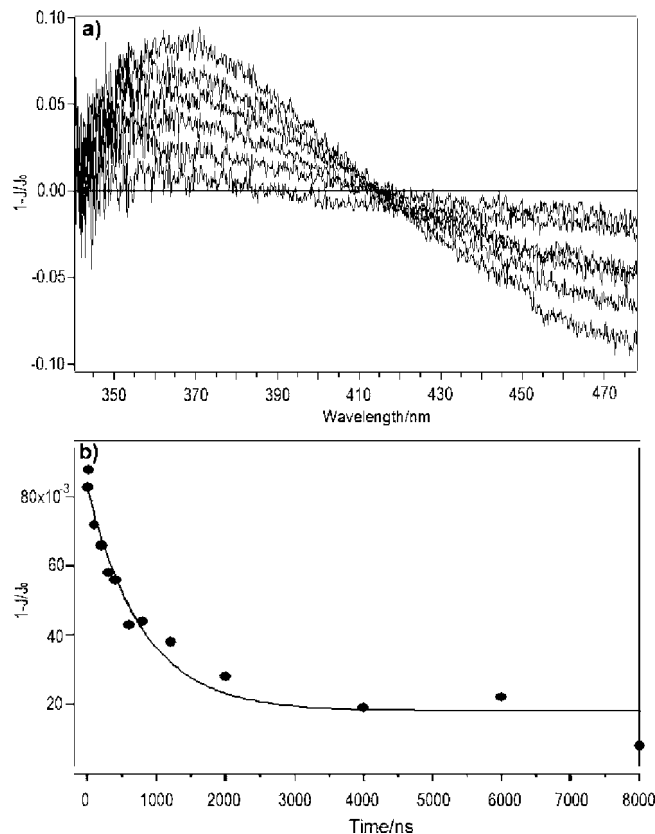


**Figure 5.** (a) Transient diffuse reflectance spectra of  $[(bpy)_2RuLDQ]^{4+}$ /zeoliteY (excitation at 458 nm, traces at 150, 350, 550, 750, 6150, and 8150 ns). (b) The decay of the intensity at 370 nm along with the monoexponential fit (solid line) of 796 ns.

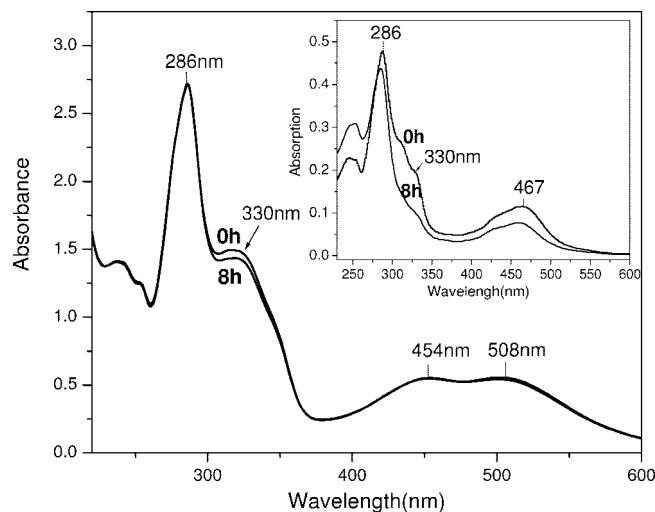


**Figure 6.** UV–vis absorption spectra of  $[(bpy)_2RuLDQ]^{4+}$  before and after 8 h light irradiation ( $\lambda > 430\text{nm}$ ) in aqueous solution. (Inset shows the UV–vis spectra of  $[(bpy)_2RuL]^{2+}$  before and after 8 h light irradiation under the same conditions).

slow phase, which extends to milliseconds. The bleach of the MLCT band shows comparable behavior, though because of the laser interference (458 nm excitation) at short delay times, we could not treat this data quantitatively.

## Discussion

**Excited State of  $[(bpy)_2RuL]^{2+}$  and  $[(bpy)_2RuLDQ]^{4+}$ .** In  $[(bpy)_2RuL]^{2+}$ , electrochemical studies show that L is more easily reduced than bpy and transient absorption studies measured

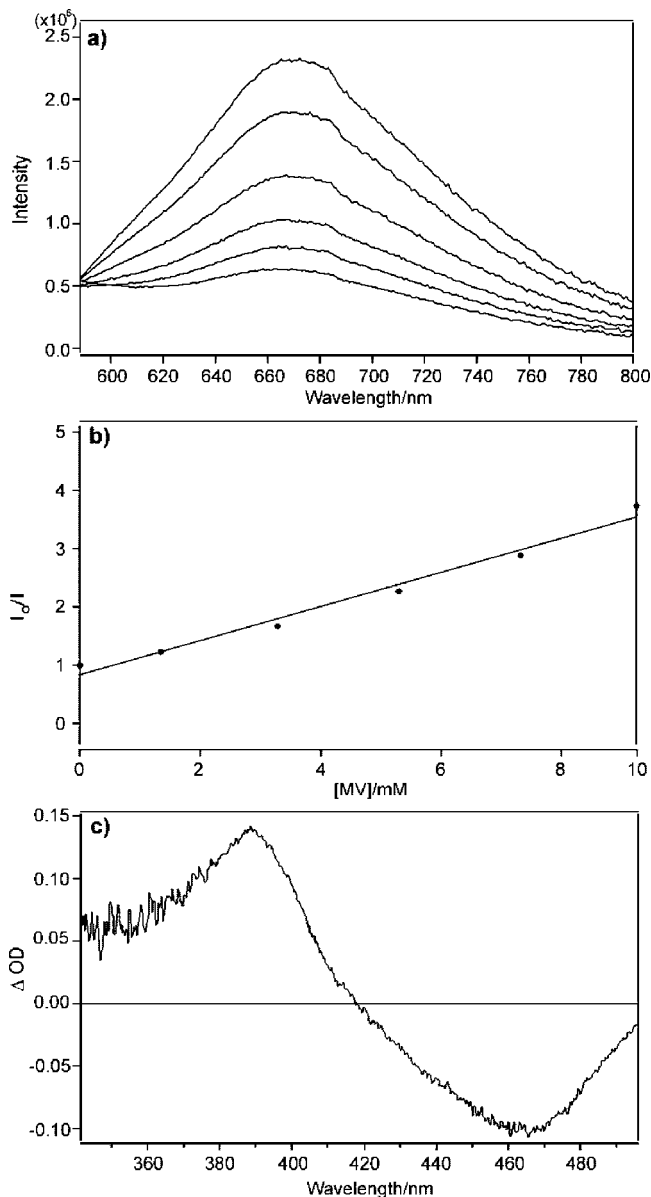


**Figure 7.** (a) Emission quenching of  $[(bpy)_2RuL]^{2+}$  ( $1 \times 10^{-5}$  M) with  $MV^{2+}$  (0, 1.34, 3.28, 5.29, 7.31, and 9.24 mM) in  $CH_3CN$ . (b) Stern–Volmer plot, (c) transient spectrum at 150 ns ( $[(bpy)_2RuL]^{2+}$  ( $1 \times 10^{-5}$  M),  $MV^{2+}$  (30 mM), excitation at 532 nm).

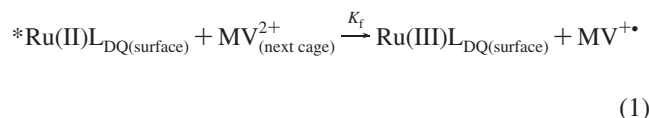
in acetonitrile have confirmed that L has radical anion character in the excited state.<sup>12</sup> Therefore, for the  $[(bpy)_2RuL]^{2+}$  complex, it is proposed that the MLCT excitation leads to electron delocalization across the olefinic ligand. Because the excited electron is delocalized on L ligand, the  $\pi^*$  ligand orbital is stabilized which results in a decreased energy gap. This explains the significant red-shift in the emission spectra of  $[(bpy)_2RuL]^{2+}$  (675 nm) as compared to that of  $[Ru(bpy)_3]^{2+}$  (620 nm).

We have reported that electron delocalization on L in  $[(bpy)_2RuL]^{2+}$  leads to photochemical instability under visible light irradiation at neutral and basic pH.<sup>14</sup> However, these photoreactions were inhibited by protonation of the free bipyridyl part of ligand L and were explained as arising from an intramolecular electron transfer to the protonated bipyridine part of L and formation of a viologen-like electron acceptor. With quaternization of the two nitrogens on bpy,  $[(bpy)_2RuL_{DQ}]^{4+}$  shows good photostability toward visible light in aqueous solutions. No significant spectroscopic changes were observed in absorption and emission after 8 h of irradiation

(Figure 6). This is because quaternization leads to the formation of a DQ moiety which is a good electron acceptor.<sup>14,30</sup> Thus, upon photoexcitation of  $[(bpy)_2RuL_{DQ}]^{4+}$ , we propose that rapid intramolecular electron-transfer to the DQ part of  $L_{DQ}$  takes place, leading to quenching of the excited state.

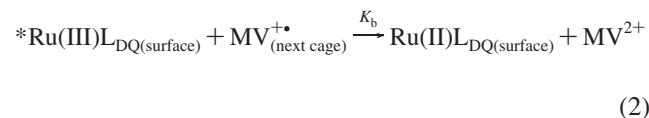
**Photoinduced Electron Transfer.** The photoinduced electron transfer from  $[(bpy)_2RuL]^{2+}$  and  $[(bpy)_2RuL_{DQ}]^{4+}$  to  $MV^{2+}$  in solution shows profound differences. For the  $[(bpy)_2RuL]^{2+}/MV^{2+}$  system,  $Ru^{III}$  species and  $MV^{+\bullet}$  are generated upon photoexcitation (Figure 7). The quenching rate constant was  $4.2 \times 10^8$  L mol<sup>-1</sup> s<sup>-1</sup>, and consistent with previous studies of  $Ru(bpy)_3^{2+}$  and viologen.<sup>31,32</sup>

The electron transfer between  $[(bpy)_2RuL_{DQ}]^{4+}$  and  $MV^{2+}$  in solution was not observable by nanosecond laser flash photolysis. For covalently connected  $Ru(bpy)_3^{2+}/linker/DQ$  systems reported in the literature, the rate constants for the intramolecular back electron transfer reaction are comparable or faster than the forward electron transfer with rate constants  $> 10^9$  s<sup>-1</sup>.<sup>22,33</sup> Once  $[(bpy)_2RuL_{DQ}]^{4+}$  is anchored on the surface of the zeolite, its excited-state properties are altered. First, emission is observed from the excited-state with a lifetime of 796 ns, indicating that once in the zeolite, intramolecular electron transfer quenching by DQ part of  $L_{DQ}$  is not observed. A possible explanation is that in the zeolite, the DQ part of the ligand is sterically constrained and cannot assume the planar form necessary for the DQ<sup>+</sup> radical and thus the intramolecular electron transfer is inhibited. Electron transfer is, however, observed from  $[(bpy)_2RuL_{DQ}]^{4+}$  on the zeolite surface to  $MV^{2+}$  within the zeolite cages (Figure 8). In the  $[(bpy)_2RuL_{DQ}]^{4+}/MV^{2+}/zeolite$ , the arrangement of the supercages and the complete filling of supercages by  $MV^{2+}$  forces the  $L_{DQ}$  and  $MV^{2+}$  to be close proximity, thereby promoting the intermolecular electron transfer from the  $L_{DQ}$  to a neighboring  $MV^{2+}$ . The driving force for the forward electron transfer is 250 mV ( $[(bpy)_2Ru^{II}L_{DQ}]^{4+*}/[(bpy)_2Ru^{III}L_{DQ}]^{5+} = -0.69$  V (using  $E_{00} = 2$  eV from emission spectrum).<sup>22</sup> Due to the highly packed  $MV^{2+}$  ( $\sim 1.5$   $MV^{2+}$ /supercage), the diffusional contribution to electron-transfer quenching is expected to be small, promoting static quenching between surface  $[(bpy)_2RuL_{DQ}]^{4+}$  and  $MV^{2+}$  in the neighboring supercages (eq 1).

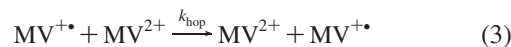


Within 100 ns of the laser pulse, the signal for  $MV^{+\bullet}$  has reached its peak, indicating that the rate constant for intermolecular quenching ( $k_f$ ) is  $> 10^7$  s<sup>-1</sup>.

The kinetic model for analyzing the decay of the  $MV^{+\bullet}$  involved two processes, the back electron transfer from the  $MV^{+\bullet}$  to  $[(bpy)_2Ru^{III}L_{DQ}]^{5+}$  ( $k_b$ , eq 2) and self-exchange of the electron between  $MV^{+\bullet}$  and  $MV^{2+}$  in neighboring supercages ( $k_{hop}$ , eq 3).



The electron hopping between neighboring  $MV^{2+}$  (eq 3) provides a pathway for the electron to move further into the zeolite.



The decay of the  $MV^{+\bullet}$  radical was fit using eqs 2 and 3 using a model based on the structure of zeolite Y. For zeolite

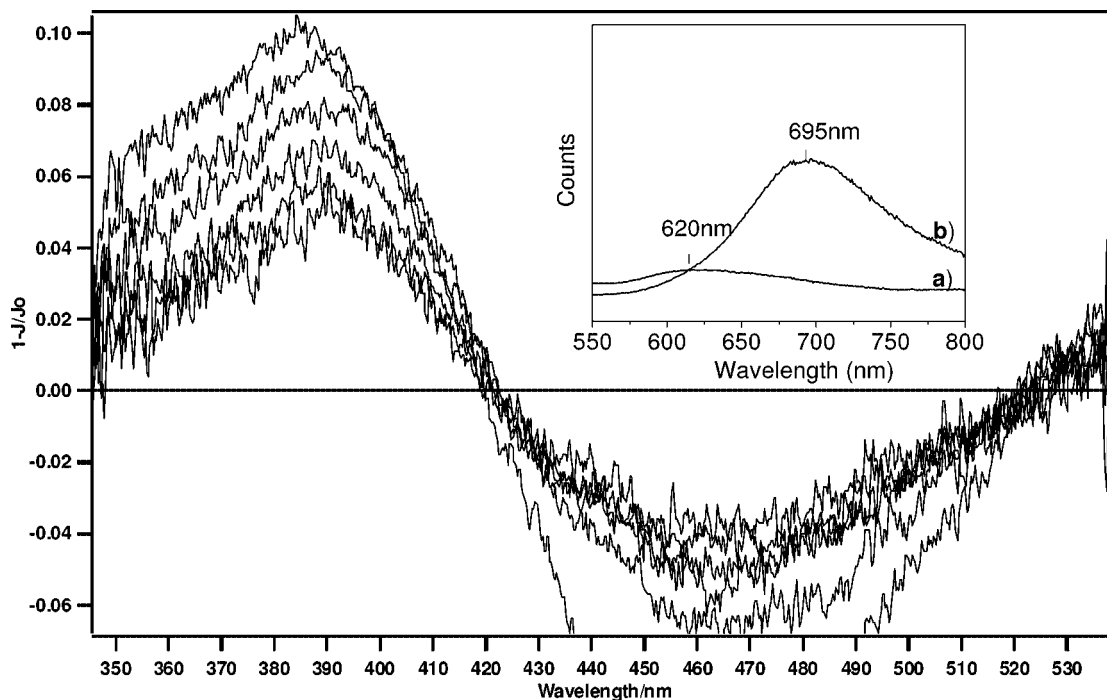


**Figure 8.** Transient diffuse reflectance spectra of  $[(bpy)_2RuLDQ]^{4+}/MV^{2+}/zeolite$  (150 ns, 650 ns, 1150 ns, 10150 ns, 50150 ns, and 1 ms), excitation at 458 nm (15 ns pulse, leaks through the detection system at 150 ns). Inset shows (a) emission quenching of  $[(bpy)_2RuLDQ]^{4+}$  by  $MV^{2+}$  (1.5 per supercage) and (b) emission of  $[(bpy)_2RuLDQ]^{4+}$  without any  $MV^{2+}$  in zeolite.

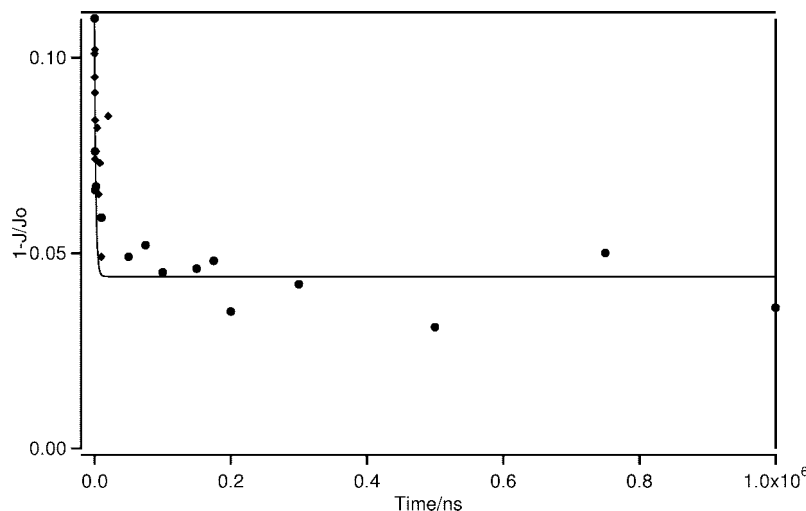


**Figure 9.** Plot of the intensity at 390 nm from Figure 8 as a function of delay time. Solid line fit with  $k_h = 2 \times 10^5 \text{ s}^{-1}$  and  $k_b = 3 \times 10^5 \text{ s}^{-1}$ .

Y, the supercages are arranged in a tetrahedral geometry, as depicted in Figure 10. Using the Stella program, a kinetic model was set up to assess the decay of the  $MV^{2+}$  using three  $k_b$ 's (each with 33.3% weight) and  $k_{hop}$ . The best fit was with the model in which the three  $k_b$ 's were assigned the same value, reflecting the positioning of the Ru-bpy unit on the zeolite surface, such that the Ru center to the three supercages containing the  $MV^{2+}$  were of similar distance. The initial value for  $k_{hop}$  ( $2.5 \times 10^5 \text{ s}^{-1}$ ) was chosen from an earlier study of a completely intrazeolitic  $[Ru(bpy)_3]^{2+}/MV^{2+}$  system.<sup>10</sup> The values of  $k_b$  and  $k_{hop}$  were adjusted, and the best fit was obtained (Figure 9) with  $k_b = 3.0 \times 10^5 \text{ s}^{-1}$  and  $k_{hop} = 2.0 \times 10^5 \text{ s}^{-1}$ .

Charge-exchange by hopping on surface of zeolite was estimated to be  $\sim 10^7 \text{ s}^{-1}$  for a  $[Ru(bpy)_3]^{2+}/linker/MV^{2+}$  exchanged on the zeolite surface.<sup>34</sup> In the present study, the loading level of  $MV^{2+}$  is higher (1.5  $MV^{2+}$  per supercage), and thus, the increased  $k_{hop}$  of  $2.0 \times 10^5 \text{ s}^{-1}$  is reasonable. For the

completely intrazeolitic case, the loading level of  $MV^{2+}$  (1.7  $MV^{2+}$  per supercage) was slightly higher and a  $k_{hop}$  of  $2.5 \times 10^5 \text{ s}^{-1}$  was used.<sup>10</sup>

The details of the mechanism of the back electron transfer and the role of the zeolite are not well understood. However, studies that have explored the electron transfer dynamics within zeolites have consistently found a slowing of the back electron transfer. Several studies have explored the transient spectroscopy of covalently held  $[Ru(bpy)_3]^{2+}/linker/nDQ^{2+}$  and  $[Ru(bpy)_3]^{2+}/linker/MV^{2+}$  ion-exchanged onto zeolite surface.<sup>34,35</sup> The attachment of  $[Ru(bpy)_3]^{2+}/linker/nDQ^{2+}$  and  $[Ru(bpy)_3]^{2+}/linker/MV^{2+}$  to the zeolite was done via ion-exchange and resembles the  $[(bpy)_2RuLH]^{3+}$  attachment shown in Scheme 1. In contrast to the molecule  $[(bpy)_2RuLDQ]^{4+}$ , the attachment in  $[Ru(bpy)_3]^{2+}/linker/nDQ^{2+}$  and  $[Ru(bpy)_3]^{2+}/linker/MV^{2+}$  was with flexible methylene or amide bridges. With the  $[Ru(bpy)_3]^{2+}/linker/nDQ^{2+}$  ion-exchanged onto a benzylviologen ( $BV^{2+}$ ) zeolite L, the back

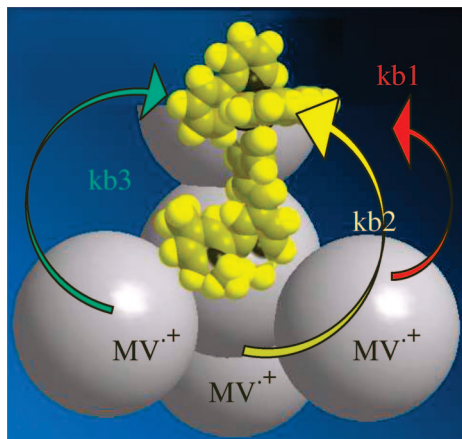


**Figure 10.** Model depicting the arrangement of  $[(bpy)_2RuL_{DQ}]^{4+}$  in a tetrahedral geometry of  $MV^{2+}$ -containing zeolite supercages.

electron transfer from  $BV^{+}$  to  $Ru^{3+}$  was found to be  $2.7 \times 10^4 \text{ s}^{-1}$ .<sup>35</sup> In another study involving  $[Ru(bpy)_3]^{2+}/linker/MV^{2+}$  ion-exchanged on the surface of the zeolite, the back electron transfer was considerably slower on the zeolite as compared to solution, leading to long-lived charge-separated states with lifetimes of hundreds of microseconds.<sup>33</sup> The longer lived charge separated state on the zeolite was explained as arising from lateral intermolecular charge separation ( $\sim 10^7 \text{ s}^{-1}$ ) competing with the back electron transfer. The decay of the  $MV^{+}$  was fit with the Albery model and an “average” back electron transfer rate constant in the range of  $10^4$ – $10^5 \text{ s}^{-1}$  was obtained, depending on the linker length, with the highest rate approaching  $4.8 \times 10^5 \text{ s}^{-1}$ .<sup>34</sup> The heterogeneity of the rates was explained as rising from conformational differences of the complex on the zeolite surface.

The rigid entrapment of the molecules and their spatial orientation and lack of conformational flexibility must play a role in the slowing of the back electron transfer reaction in the zeolite. Also, in the zeolite, the possibility of  $k_{hop}$  and its comparable magnitude to  $k_b$ , leads to long-lived charge separated states. Intrazeolitic space with ion-exchanged  $MV^{2+}$  also resembles a frozen medium. The “bulk-like” water molecules in the supercages are replaced by the  $MV^{2+}$  and remaining water is held by the framework and  $Na^+$  ions. Thus, reorganization of the solvent molecules within the supercages following electron transfer will be severely limited. Previous studies of electron transfer in frozen media have shown that back electron transfer is slowed down.<sup>36,37</sup>

Quantum efficiency of charge separation can be estimated with the following assumptions.<sup>8,10</sup> At time  $t = 0$ , from Figures 5 and 8, we can estimate a diffuse reflectance ( $1 - J/J_0$ ) signal for  $[(bpy)_2RuL_{DQ}]^{4+}$  and  $MV^{+}$  to be 0.088 and 0.098 (average of three experiments), respectively. These signals should be proportional to concentrations of these species (comparable to absorbances), with the molar extinction coefficient being the proportionality constants, since the same zeolite sample is used in both experiments. The molar extinction coefficient for  $MV^{+}$  is  $4.2 \times 10^4$ , and if we approximate the molar extinction coefficient of  $[(bpy)_2RuL_{DQ}]^{4+}$  to be that of  $[(bpy)_3Ru]^{2+}$  ( $2.7 \times 10^4$ ), then the quantum yield of initial charge separation is 70%. Since about 40% of the  $MV^{+}$  is observed at times greater than 100  $\mu\text{s}$  (Figure 9), the overall yield of usable charge-separated species is 30%. Estimates for quantum yields for charge separation for a completely intrazeolitic  $[Ru(bpy)_3]^{2+}$  surrounded by bipyridinium ions was between 44% and 59%.<sup>10</sup> For  $[Ru(bpy)_3]^{2+}$  ion exchanged on the surface of a  $MV^{2+}$ -

exchanged zeolite, the quantum yield for charge separation was estimated at 7%.<sup>8</sup> When covalently linked  $[Ru(bpy)_3]^{2+}/linker/viologen$  units were ion-exchanged into zeolite via the viologen unit, the quantum yields for charge separation were in the 5–7% range.<sup>34</sup> The quantum yield for charge separation ( $Ru^{3+}/BV^{+}$ ) for a  $[Ru(bpy)_3]^{2+}/linker/DQ$  exchanged onto the surface of the benzylviologen ( $BV^{2+}$ ) exchanged zeolite L was found to be  $17 \pm 5\%$ .<sup>35</sup> One of the possible reasons for considerably higher value of the quantum yield (70%) in the present study is the use of zeolite Y which ensures that the  $L_{DQ}$  is surrounded by three supercages with  $MV^{2+}$ , while the  $Ru^{2+}/BV^{2+}$  study was done with zeolite L, a one-dimensional zeolite.

The longer-lived charge-separated species, as well as electron migration into the zeolite via hopping of the electron via the viologens, is consistent with our steady-state photolysis studies, where we have shown that upon photoexcitation of  $[(bpy)_2RuL_{DQ}]^{4+}$  bound to a zeolite membrane surface, charge was propagated through the membrane by the intrazeolitic bipyridinium ions to the opposite side of the membrane.<sup>16</sup> The high efficiency of charge transport through the membrane in the steady state studies is related to the slow back electron transfer and the electron hopping, which is concluded from the spectroscopic studies in this paper.

**Acknowledgment.** We acknowledge funding from the DOE Office of Basic Energy Sciences (DE-FG02-06ER15776).

**Supporting Information Available:** Additional figures. This material is available free of charge via the Internet at <http://pubs.acs.org>.

## References and Notes

- (1) Bard, A. J.; Fox, M. A. *Acc. Chem. Res.* **1995**, *28*, 141–145.
- (2) Graetzel, M.; Kalyanasundaram, K. *Surfactant Science Series, Vol. 38: Kinetics and Catalysis in Microheterogeneous Systems*. **1991**, 525.
- (3) Thomas, J. K.; Hashimoto, S. *New J. Chem.* **1987**, *11*, 145–149.
- (4) Dutta, P. K.; Ledney, M. *Prog. Inorg. Chem.* **1997**, *44*, 209–271.
- (5) Kalyanasundaram, K. In *Photochemistry of polypyridine and porphyrin complexes*; Academic Press: London; San Diego, 1992.
- (6) Borja, M.; Dutta, P. K. *Nature* **1993**, *362*, 43–45.
- (7) Sykora, M.; Kincaid, J. R. *Nature* **1997**, *387*, 162–164.
- (8) Kim, Y. I.; Mallouk, T. E. *J. Phys. Chem.* **1992**, *96*, 2879.
- (9) Castagnola, N. B.; Dutta, P. K. *J. Phys. Chem. B* **1998**, *102*, 1696–1702.
- (10) Vitale, M.; Castagnola, N. B.; Ortins, N. J.; Brooke, J. A.; Vaidyalngam, A.; Dutta, P. K. *J. Phys. Chem. B* **1999**, *103*, 2408–2416.
- (11) Juris, A.; Balzani, V.; Barigelli, F.; Campagna, S.; Belser, P.; von Zelewsky, A. *Coord. Chem. Rev.* **1988**, *84*, 85–277.
- (12) Strouse, G. F.; Schoonover, J. R.; Duesing, R.; Boyde, S.; Jones, W. E., Jr; Meyer, T. J. *Inorg. Chem.* **1995**, *34*, 473–487.
- (13) Shaw, J. R.; Webb, R. T.; Schmehl, R. H. *J. Am. Chem. Soc.* **1990**, *112*, 1117–1123.
- (14) Zhang, H.; Rajesh, C. S.; Dutta, P. K. *J. Phys. Chem. A* **2008**, *112*, 808–817.
- (15) Kim, Y.; Lee, H.; Dutta, P. K.; Das, A. *Inorg. Chem.* **2003**, *42*, 4215–4222.
- (16) Kim, Y.; Das, A.; Zhang, H.; Dutta, P. K. *J. Phys. Chem. B* **2005**, *109*, 6929–6932.
- (17) Beard, C. D.; Baum, K.; Grakauskas, V. *J. Org. Chem.* **1973**, *38*, 3673–3677.
- (18) Homer, R. F.; Tomlinson, T. E. *J. Chem. Soc.* **1960**, 2498–2503.
- (19) Pirzada, N. H.; Pojer, P. M.; Summers, L. A. *Z. Naturforsch., Teil B: Anorg. Chem., Org. Chem.* **1976**, *31B*, 115–121.
- (20) Elliott, C. M.; Freitag, R. A. *J. Chem. Soc., Chem. Commun.* **1985**, 156–157.
- (21) Elliott, C. M.; Freitag, R. A.; Blaney, D. D. *J. Am. Chem. Soc.* **1985**, *107*, 4647–4655.
- (22) Cooley, L. F.; Headford, C. E. L.; Elliott, C. M.; Kelley, D. F. *J. Am. Chem. Soc.* **1988**, *110*, 6673–6682.
- (23) Coe, B. J.; Curati, N. R. M.; Fitzgerald, E. C. *Synthesis* **2006**, 146–150.
- (24) Shepherd, R. E.; Slocik, J. M.; Stringfield, T. W.; Somayajula, K. V.; Amoscato, A. A. *Inorg. Chim. Acta* **2004**, *357*, 965–979.

- (25) Arakawa, R.; Matsuda, F.; Matsubayashi, G.; Matsuo, T. *J. Am. Soc. Mass Spectrom.* **1997**, *8*, 713–717.
- (26) Schoeman, B. J.; Sterte, J.; Otterstedt, J. E. *Zeolites* **1994**, *14*, 110–116.
- (27) Lechert, H.; Kacirek, H. *Zeolites* **1991**, *11*, 720–728.
- (28) Den Ouden, C. J. J.; Thompson, R. W. *J. Colloid Interface Sci.* **1991**, *143*, 77–84.
- (29) Thompson, A. M. W. C.; Smailes, M. C. C.; Jeffery, J. C.; Ward, M. D. *J. Chem. Soc., Dalton Trans.* **1997**, 737–743.
- (30) Guardigli, M.; Flamigni, L.; Barigelletti, F.; Richards, C. S. W.; Ward, M. D. *J. Phys. Chem.* **1996**, *100*, 10620–10628.
- (31) Prasad, D. R.; Mandal, K.; Hoffman, M. Z. *Coord. Chem. Rev.* **1985**, *64*, 175–190.
- (32) Kelly, L. A.; Rodgers, M. A. J. *J. Phys. Chem.* **1995**, *99*, 13132–13140.
- (33) Yonemoto, E. H.; Riley, R. L.; Kim, Y. I.; Atherton, S. J.; Schmehl, R. H.; Mallouk, T. E. *J. Am. Chem. Soc.* **1992**, *114*, 8081–8087.
- (34) Yonemoto, E. H.; Kim, Y. I.; Schmehl, R. H.; Wallin, J. O.; Shoulders, B. A.; Richardson, B. R.; Haw, J. F.; Mallouk, T. E. *J. Am. Chem. Soc.* **1994**, *116*, 10557–10563.
- (35) Krueger, J. S.; Mayer, J. E.; Mallouk, T. E. *J. Am. Chem. Soc.* **1988**, *110*, 8232–8234.
- (36) Jones, W. E., Jr.; Chen, P.; Meyer, T. J. *J. Am. Chem. Soc.* **1992**, *114*, 387–388.
- (37) Chen, P.; Meyer, T. J. *Inorg. Chem.* **1996**, *35*, 5520–5524.

JP8061459